Nanoscale Advances

ROYAL SOCIETY OF CHEMISTRY

PAPER

View Article Online
View Journal | View Issue

Cite this: *Nanoscale Adv.*, 2026, **8**, 2021

Nitrogen cavitation enables rapid and high-yield preparation of functional cell-membrane-derived vesicles

Changting Li,†*[ab] Dehua Luo,†[a] Can Peng,[a] Qun Luo,[a] Wenjing Xu,[c] Jincheng Zhou,[a] Wen Su,[c] Wei Wu[d] and Yi-Feng Wang *[a]

Cell-membrane-derived vesicles (CMDVs) are increasingly utilized for the delivery of bioactive molecules due to their retention of membrane proteins, low immunogenicity, and biocompatibility. However, existing preparation methods (such as homogenization, sonication, and extrusion) struggle to strike a balance between scalability and structural integrity. More importantly, these methods lack subcellular selectivity, often leading to contamination from nuclei, mitochondria, lysosomes, and peroxisomes, which compromises the purity of the vesicles. Here, we present an optimized nitrogen cavitation-based workflow for the CMDV preparation within <2 hours. Using nanoluciferase-expressing HEK 293 cells (HEK 293_NLuc), we validated that this method is highly robust, allowing for successful CMDV generation under varying cell densities and pressures, as well as under high viscosity and salt conditions, with uniform particle size, minimal contamination, and preserved membrane-associated bioactivity. Functional assays confirmed enhanced cytotoxic T lymphocyte (CTL) cytotoxicity and enzymatic retention. This method offers a rapid, scalable, and function-preserving platform for CMDV production, enabling broad applications in drug delivery, immunotherapy, and biomimetic system design.

Received 4th September 2025
Accepted 19th January 2026

DOI: 10.1039/d5na00855g

rsc.li/nanoscale-advances

Introduction

Membrane vesicles constitute a broad family of lipid bilayer nanoparticles originating from either endogenous biogenesis pathways or controlled physicochemical processing. This category includes extracellular vesicles (EVs),[1–3] such as exosomes derived from the endosomal MVB pathway, and microvesicles shed directly from the plasma membrane, as well as engineered vesicles such as cell-membrane-derived vesicles (CMDVs)[4–6] and cell-bound membrane vesicles (CBMVs).[7,8] Despite their distinct origins, these vesicles preserve key membrane features of the parent cell, including protein topology, lipid-raft organization, and receptor presentation, enabling intercellular communication and cargo transfer. EVs have been widely explored for diagnostics and therapy; however, their natural secretion is intrinsically low, and current isolation approaches (ultracentrifugation, density gradients, SEC) remain labor-intensive, low-throughput, and difficult to scale.[9,10] Many of these techniques also risk compromising EV integrity, bioactivity, or purity, especially when large volumes are processed.[11,12] These limitations create a bottleneck for producing EVs at sufficient yield, purity, and reproducibility for translational applications.[13,14]

To address these limitations, artificially generated CMDVs have emerged as a rapidly advancing class of engineered membrane vesicles that reproduce the surface architecture, membrane topology, and receptor repertoires of their parental cells while enabling precisely tunable, high-yield production.[5,6,15] Similar to EVs, these CMDVs inherit the surface function of their parent cells, conferring superior biocompatibility, low immunogenicity, and long circulation time.[16,17] Existing fabrication methods (such as mechanical extrusion, probe sonication, freeze–thaw cycling, or high-pressure homogenization) can disrupt the plasma membrane but often at the cost of extensive nanodomain disorganization, uncontrolled heat generation, and non-selective rupture of intracellular organelles. This leads to contamination by nuclear DNA, histones, lysosomal hydrolases, or mitochondrial DAMPs, all of which compromise vesicle purity, immunological safety, and functional reproducibility.[10,18–20] Therefore, an ideal method for producing CMDVs must simultaneously achieve high processing efficiency, structural selectivity, preservation of membrane-associated functional proteins, minimization of subcellular contamination (such as nuclear envelope or organelle-derived components), and scalability for reproducible manufacturing.

[a]*Guangzhou Institute of Cancer Research, The Affiliated Cancer Hospital, School of Biomedical Engineering, Guangzhou Medical University, Guangzhou 510260, Guangdong, P. R. China. E-mail: lichangtingcurie@gmail.com; yifengwang91@gmail.com*

[b]*NewShell VesicleTech of Institut Baulieu, Paris 94270, France*

[c]*Department of Pathology, Shenzhen University, Shenzhen 518060, China*

[d]*Cancer Center, The First Hospital of Jilin University, Changchun 130021, China*

† These authors contributed equally to this work.

Nitrogen cavitation offers a gentler and more uniform mechanical disruption strategy compared to conventional methods and was originally developed for subcellular fractionation.[21–23] In nitrogen cavitation, cells are equilibrated with inert nitrogen gas under a defined pressure, allowing nitrogen to dissolve into the cytosol and intermembrane spaces. Rapid decompression triggers sub-millisecond adiabatic expansion of intracellular microbubbles, generating intense local shear forces and transient transmembrane pressure gradients. At the moment of release, the extracellular pressure drops to atmospheric levels while the intracellular compartment remains at the pre-set saturation pressure, mechanically rupturing the plasma membrane before cytoskeletal or membrane–protein complexes can reorganize to dissipate the stress.[24] Unlike static overpressure lysis, nitrogen cavitation produces localized shear fields that perforate and vesiculate membranes without uniform crushing, while adiabatic cooling (Joule–Thomson effect) mitigates thermal denaturation, and the inert atmosphere prevents oxidative damage or detergent-induced artifacts. By adjusting the applied pressure to exploit differential rupture thresholds between organelles, this method enables selective disruption of target membranes while preserving the integrity of more resilient subcellular structures. Consequently, membrane morphology and protein integrity are preserved more effectively than with chemical lysis or sonication.[22,25]

Although previously applied for organelle isolation, its use in generating CMDVs from whole cells has remained underexplored. In our prior studies, we demonstrated that nitrogen cavitation, under detergent-free conditions, could successfully release functional membrane proteins, such as interferon-γ receptor (IFN-γR), from intact cells.[26] This confirmed the method's ability to preserve sensitive transmembrane protein conformation and supports the core premise of the present invention: a shear-based vesicle generation platform that combines structural selectivity with biofunction retention. Here, we investigate nitrogen cavitation as a rapid, scalable, and function-preserving method to prepare CMDVs derived from HEK 293_NLuc cells ($CMDVs^{HEK\ 293\_NLuc}$) and CTL ($CMDVs^{CTL}$) within <2 hours. We provide an integrated evaluation of physical and chemical properties, organelle contamination, functional retention, including immune effector enhancement, and enzymatic activity.

Materials and methods

Cell lines and culture conditions

CTLs were maintained in RPMI-1640 supplemented with 10% fetal bovine serum (FBS) and 10 ng per mL IL-2. HEK 293_NLuc cells were maintained in DMEM supplemented with 10% FBS. Cells were grown at 37 °C under 5% CO_2 and harvested at 70–80% confluence. Before CMDV production, cells were washed twice with PBS and counted using a hemocytometer.

Nitrogen cavitation

Washed cells were resuspended in hypotonic lysis buffer (10 mM HEPES, pH 7.4, 10 mM KCl, 1.5 mM $MgCl_2$) at a concentration of 5×10^6 cells per mL and incubated on ice for 10 minutes. Then, cell suspensions were transferred to a nitrogen cavitation bomb (Parr Instrument Company), pressurized to different pressures (300, 450, 600 psi) with N_2 gas, and incubated for 10 minutes at 4 °C. The pressure was then rapidly released to induce cavitation and membrane rupture. To assess the robustness of this method, HEK 293_NLuc cells were also resuspended at a high density (2.5×10^7 cells per mL) and in different buffers (350 mM sucrose and 300 mM NaCl). Subsequently, the CMDVs were prepared according to the aforementioned method, maintaining the pressure at 300 psi. For each set of preparation conditions, CMDV preparation was conducted in at least three batches.

Centrifugation-based CMDV enrichment

Post-cavitation lysates were subjected to stepwise centrifugation at 4 °C to fractionate cellular components: 1000 × *g* for 10 minutes to remove nuclei and large debris, followed by 10 000 × *g* for 45 minutes to eliminate mitochondria, lysosomes, and other dense organelles. Depending on the intended application and purity requirements, an additional ultracentrifugation step was optionally performed twice at 160 000 × *g* for 90 and 120 minutes to collect highly purified CMDVs. This step was conducted using a Beckman Coulter Optima XPN-100 ultracentrifuge with a SW32Ti rotor and was primarily used for downstream applications requiring high structural homogeneity and minimal contaminants, such as membrane protein analysis or therapeutic vesicle formulations.

Physicochemical properties and morphological characterization of CMDVs

Size distribution and concentration of CMDVs were measured by nanoparticle tracking analysis (NTA, Particle Metrix, Germany). The sample was diluted with ultrapure water according to its concentration, and injected into the detection pipeline at a constant speed using a 1 mL syringe. When the instrument detects a particle count of 50–200 in the preview field, CMDV concentration and size were detected and analyzed. The zeta potential of the CMDVs was characterized using dynamic light scattering (DLS, Zetasizer Ultra, United Kingdom). For transmission electron microscopy (TEM) imaging, 10 μL of the CMDV suspension was dropped onto a clean 200 mesh carbon-coated grid (cat no. BZ11022a, Zhongjing Technology). The copper grid was placed face down onto the CMDVs, allowing adsorption for 10 minutes. The grid was then dried and stained with 3% uranyl acetate for 1.5 minutes. Then, the CMDVs on the copper grid were observed using a JEM-1400 Plus TEM at 80 kV. Images were captured using the RADIUS software.

Purity characterization of CMDVs

Western blotting was performed to detect the organelle protein marker in CMDVs. The CMDVs were lysed using 10× RIPA buffer, and the protein extracts were separated by 4–12% gradient SDS-PAGE, followed by the transfer of proteins onto a PVDF membrane using a 100 V. After blocking with 5% skim milk for 60 minutes, the membrane was incubated separately

with anti-EEA1 antibody (BD Biosciences, cat no. 610457), anti-calnexin antibody (Abcam, cat no. ab133615), anti-nanoluciferase antibody (Promega, cat no. N700A), anti-GM130 antibody (Cell Signaling Technology, cat no. 12480T), anti-lamin B1 antibody (Proteintech, cat no. 12987-1-AP), anti-LAMP1 antibody (Abcam, cat no. ab24170), and anti-VDAC1 antibody (Abcam, cat no. ab154856). These primary antibodies were incubated overnight at 4 °C, followed by a 60 minutes incubation with the goat anti-rabbit IgG-HRP secondary antibody or rabbit anti-mouse IgG-HRP secondary antibody. The membrane was then incubated with the ECL sensitive luminescence solution for 1 minute before imaging using the gel imaging system (ChemiScope 6100, CLINX).

Theoretical vesicle yield estimation

To estimate the theoretical upper limit of vesicle yield per cell, we constructed a geometrically derived model based on surface area considerations. This model assumes that the plasma membrane serves as the predominant source of vesicle material and that the resulting vesicles are uniform (monodisperse) and spherical. Using Jurkat T cells as a representative case, given their near-spherical morphology with an average diameter of approximately 15 μm, the total available plasma membrane surface area can be calculated using the standard formula for the surface area of a sphere:

$$A_{\text{cell}} = 4\pi r^2 = 4\pi\left(\frac{15}{2}\right)^2 = 4\pi(7.5)^2 = 4\pi \times 56.25 \approx 706.86\ \mu\text{m}^2$$

The surface area of a single vesicle (A_{vesicle}) with a diameter of 125 nm (0.125 μm) is:

$$A_{\text{vesicle}} = 4\pi r^2 = 4\pi(0.0625)^2 = 4\pi \times 0.00391 \approx 0.0491\ \mu\text{m}^2$$

Assuming 100% of the cell's plasma membrane is converted into vesicles without overlap or waste, the theoretical upper limit of vesicle yield (N) per cell is:

$$N = \frac{A_{\text{cell}}}{A_{\text{vesicle}}} \approx \frac{706.86}{0.0491} \approx 14396\ \text{vesicles}$$

For the calculation of the actual vesicle yield in the experiment, the total number of obtained vesicles was divided by the total number of cells, thereby obtaining the number of vesicles produced per cell.

Enzymatic activity assay of purified CMDVs$^{\text{HEK 293_NLuc}}$

According to the Nano Glo® Live Cell Assay kit (N2011, Promega), the substrate and buffer were mixed in a ratio of 1 : 19, then the mixture was mixed with the CMDVs$^{\text{HEK 293_NLuc}}$ in a volume ratio of 1 : 5 and added to a transparent 96-well plate. The bioluminescence intensity was immediately detected by an enzyme-linked immunosorbent assay (ELISA) reader (Synergy™ H1, BioTek).

CMDVs$^{\text{CTL}}$-mediated killing assay

1000 MC38-OVA cells were seeded into a 96-well plate for 48 h. Then, hypotonic lysis buffer and CMDVs$^{\text{CTL}}$ were added to the cells and treated for 24 h, and then cell numbers were counted by FACS.

$$\text{Killing efficiency} = \frac{1 - \text{left cell number of treated well}}{\text{cell number of untreated well}} \times 100\%$$

Results and discussion

Setting up the protocol for CMDV preparation *via* nitrogen cavitation

To harvest function-preserving and minimally contaminated CMDVs, we established a protocol and optimized key steps for the preparation of CMDVs *via* nitrogen cavitation (Fig. 1).

First, we selected a mildly hypotonic buffer, specifically designed to induce gentle osmotic swelling of cells and sensitize the plasma membrane to shear-induced rupture. This low-ionic-strength formulation promotes membrane relaxation without triggering premature lysis or compromising organelle integrity. Importantly, the buffer maintains near-physiological pH and avoids the use of detergents, thereby preserving the structural integrity and bioactivity of membrane-embedded proteins.[27] The inclusion of Mg^{2+} further stabilizes nuclear and ribosomal components during disruption. In addition, the reduced ionic strength helps minimize vesicle aggregation and facilitates cleaner post-cavitation separation, contributing to improved vesicle yield and purity. Second, the optimal pressure is a key parameter for avoiding contamination from the organelle membrane. Nitrogen cavitation has been used for cell homogenization. Generally, the cell membrane, endosomes, endoplasmic reticulum (ER), and Golgi apparatus (Golgi) are composed of delicate lipid structures that readily fragment into vesicles during cavitation under applied low pressure.[28–34] In contrast, mitochondria, lysosomes, peroxisomes, and nuclei possess multilamellar or enzyme-rich membranes with high mechanical resilience, allowing them to remain structurally intact after cavitation with lower pressure.[24,31,35–37] Thus, selecting the appropriate working pressure is essential to enable controlled rupture of plasma membranes and fragile internal compartments while maintaining intact denser, mechanically robust organelles. Nitrogen gas is loaded into the cavitation chamber and equilibrated for 10 minutes on ice. Rapid decompression induces intracellular nitrogen bubble expansion, generating uniform shear forces that rupture the plasma membrane and labile internal membranes. As shown in Fig. 1, nuclei, mitochondria, and lysosomes remain structurally intact by optimizing the pressure. In contrast, cell membranes, the ER, and the Golgi are fragmented into membrane-bound vesicles.

Then, the centrifugal separation is tuned to match known organelle-specific thresholds. A 1000 × g spin removes nuclei and large debris; 10 000 × g clears mitochondria, lysosomes, and other dense organelles. For applications requiring higher purity or downstream validation, an additional

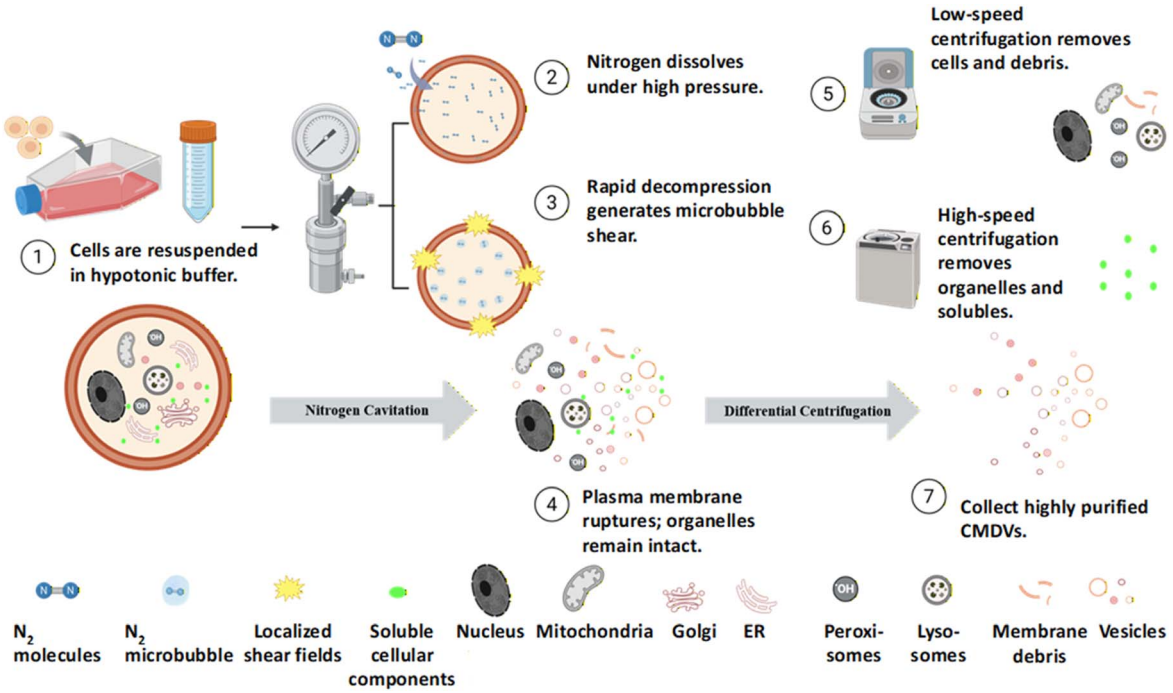

Fig. 1 Workflow of CMDV preparation *via* nitrogen cavitation. (1) Cultured cells were collected and resuspended in a mildly hypotonic buffer to increase membrane susceptibility to cavitation. (2) During pressure equilibration at a specified cavitation pressure, nitrogen gas diffuses across the plasma membrane and dissolves into both the cytosol and the lipid bilayer. (3) Rapid decompression induces intracellular microbubble nucleation and expansion, generating localized shear forces that preferentially rupture the plasma membrane while preserving mechanically robust organelles such as nuclei, mitochondria, lysosomes, and peroxisomes. Cavitation releases cytosolic contents and membrane fragments that spontaneously reseal to form CMDVs. (4) The crude lysate contains CMDVs, cytosolic proteins, membrane fragments, and intact organelles. (5) Differential centrifugation at 1000 × *g* for 10 minutes removes intact cells and nuclei. (6) A subsequent 10 000 × *g* spin for 45 minutes pellets mitochondria, lysosomes, and other dense organelles. An optional ultracentrifugation step (*e.g.*, 160 000 × *g*) was employed in this study to further purify CMDVs by removing free proteins and residual contaminants. (7) The resulting supernatant is enriched in CMDVs, which exhibit preserved membrane architecture and functional surface components. Created with Biorender.com.

ultracentrifugation step at 160 000 × *g* can be optionally performed to pellet highly purified vesicles. This step is not essential to vesicle formation but enhances structural uniformity for characterization or therapeutic use. The resulting CMDV fraction consists predominantly of small vesicles derived from the plasma membrane and disassembled internal compartments (*e.g.*, endosomes, the ER, and Golgi) with minimal contamination from intact subcellular organelles. This process design enhances product purity and ensures compositional consistency of the vesicle population. Notably, the primary advantage of this method is its capacity to enable rapid preparation and purification within <2 hours, while preserving the bioactivity of the biomolecules involved. Meanwhile, the methods can effectively mitigate the contamination by extraneous organelle components that commonly arise from manual homogenization procedures. Further, this streamlined workflow supports both scalability and reproducibility, making it well-suited for downstream functional studies and therapeutic development.

Influence of preparation conditions on the production of CMDVs

Consistent with the above discussion, nitrogen pressure is critical for the successful preparation of CMDVs. Consequently, we initially examined the influence of varying nitrogen pressures (300, 450, and 600 psi) on CMDVs$^{HEK\ 293_NLuc}$ formation. The detailed characterization of CMDVs was analyzed by NTA and TEM. As shown in Fig. 2a, NTA measurements revealed median CMDV diameters of 125 nm, 105 nm, and 106 nm, respectively, corresponding to the 300, 450, and 600 psi conditions. Zeta potential measurements showed strongly negative surface charges, ranging between −28 and −31 mV (Table 1). Furthermore, NTA data indicated an increase in the total CMDV count from 1.28×10^{11} to 1.93×10^{11} particles as the pressure was elevated from 300 to 600 psi, suggesting that higher pressure favors the production of smaller, more numerous vesicles. TEM imaging demonstrated that CMDVs derived from under different pressures shared a similar membrane integrity and cup-shaped morphology with minimal evidence of aggregation and cellular debris, or contamination from other organelles (Fig. 2b–d).

To further validate whether CMDVs are contaminated with subcellular organelles, such as mitochondria, lysosomes, and nuclei, we performed western blotting analysis using organelle-specific protein markers under increasing pressure. Western blotting confirmed effective organelle removal, showing that mitochondrial (VDAC1), nuclear (Lamin B1), and lysosomal (LAMP1) markers were nearly absent in purified CMDVs. This

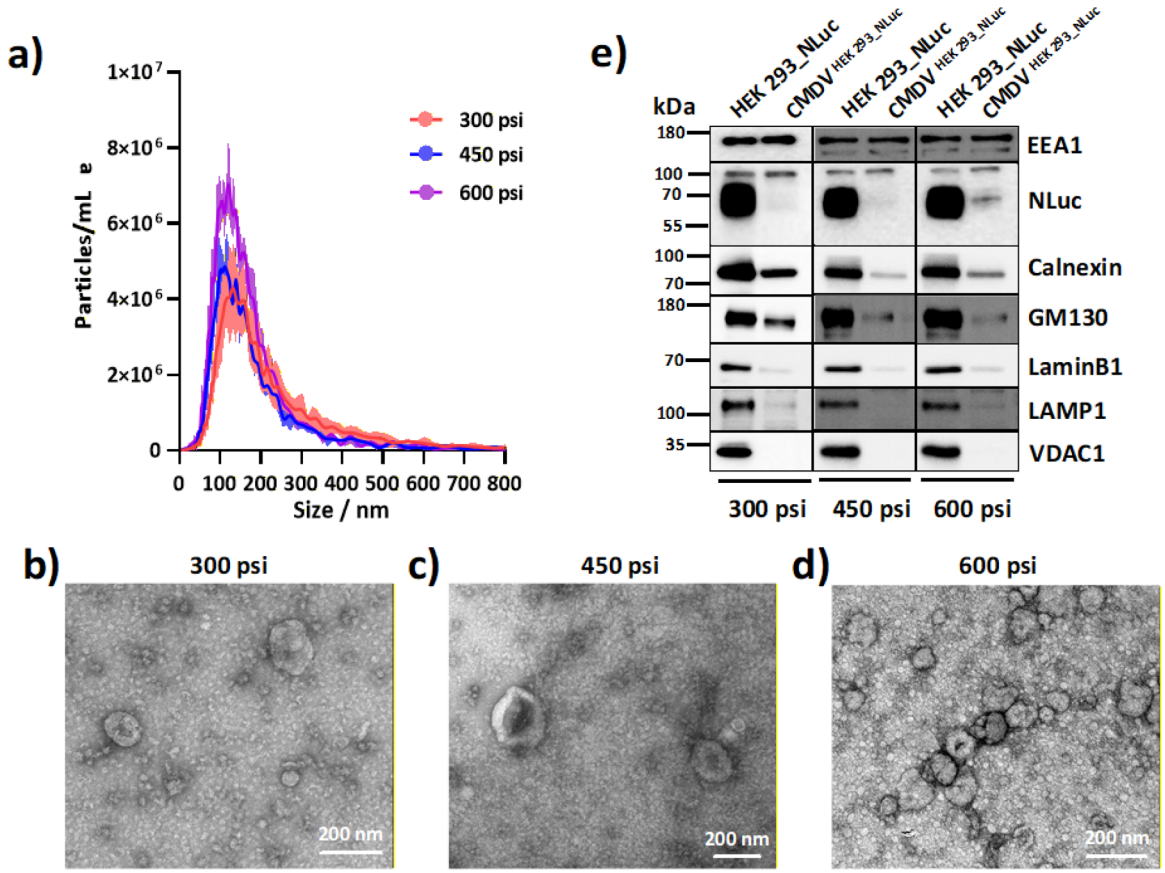

Fig. 2 Characterization of CMDVs$^{HEK\ 293_NLuc}$ produced under different pressures. (a) The size distribution of CMDVs$^{HEK\ 293_NLuc}$ produced under different pressures (300, 450, and 600 psi). (b–d) TEM imaging of (b) CMDVs$^{HEK\ 293_NLuc}$ produced under 300 psi, (c) CMDVs$^{HEK\ 293_NLuc}$ produced under 450 psi, and (d) CMDVs$^{HEK\ 293_NLuc}$ produced under 600 psi. (e) Western blotting of different organelle protein markers in CMDVs$^{HEK\ 293_NLuc}$. Endosome marker: EEA1, membrane protein: NLuc, ER marker: Calnexin, Golgi marker: GM130, nucleus marker: Lamin B1, lysosomal marker: LAMP1, mitochondrial marker: VDAC1.

suggests that robust organelles like nuclei, mitochondria, and lysosomes were successfully excluded during differential centrifugation, maintaining their integrity and separability even under the highest applied pressure (Fig. 2e). This also indicates that the pressure selection range for vesicle preparation is more flexible (it should be noted that the pressure threshold may vary depending on the cell type). For the included marker, the endosomal marker EEA1, the ER marker calnexin, the cell membrane marker CD63-NLuc, and the Golgi marker GM130 appeared in all condition groups. This suggests that the enriched vesicles mainly originate from these organelle membrane structures (Fig. 2e).

Furthermore, the influence of nitrogen cavitation may also be modulated by cell density and solution properties, as these factors can affect nitrogen permeation into cells. To test this, we prepared CMDVs at a fivefold increased cell density (2.5×10^7 cells). The results showed that the size and the zeta potential of CMDVs are 109 nm and – 40 mV, respectively (Fig. 3a and Table 1), and have classical cup-shaped morphology (Fig. 3b). Organelles with lower mechanical resistance, including endosomes, the ER, Golgi, and cell membrane, can still be assembled and detected in CMDVs, especially CMDVs derived from the Golgi were enriched compared those generated at low cell density. However, the level of contamination from the nucleus

Table 1 Physicochemical properties of CMDVs generated under different conditions

Cell line	Preparation conditions		Total number of CMDVs	Size/nm (mean ± SD)	Polydispersity index (PDI)	Zeta potential/mV (mean ± SD)
HEK 293_NLuc	Pressure	300 psi	1.28×10^{11}	125.2 ± 2.6	0.3877	−29.9 ± 8.3
		450 psi	1.40×10^{11}	105.1 ± 2.9	0.3251	−28.6 ± 12.4
		600 psi	1.93×10^{11}	105.6 ± 6.2	0.2639	−29.8 ± 4.1
	Cell density	2.5×10^7/mL	2.73×10^{11}	108.7 ± 1.8	0.2515	−40.0 ± 6.4
	Buffer	350 mM sucrose	6.83×10^{10}	119.4 ± 2.8	0.395	−28.1 ± 8.5
		300 mM NaCl	4.46×10^{10}	112.5 ± 3.9	0.2062	−31.2 ± 4.7

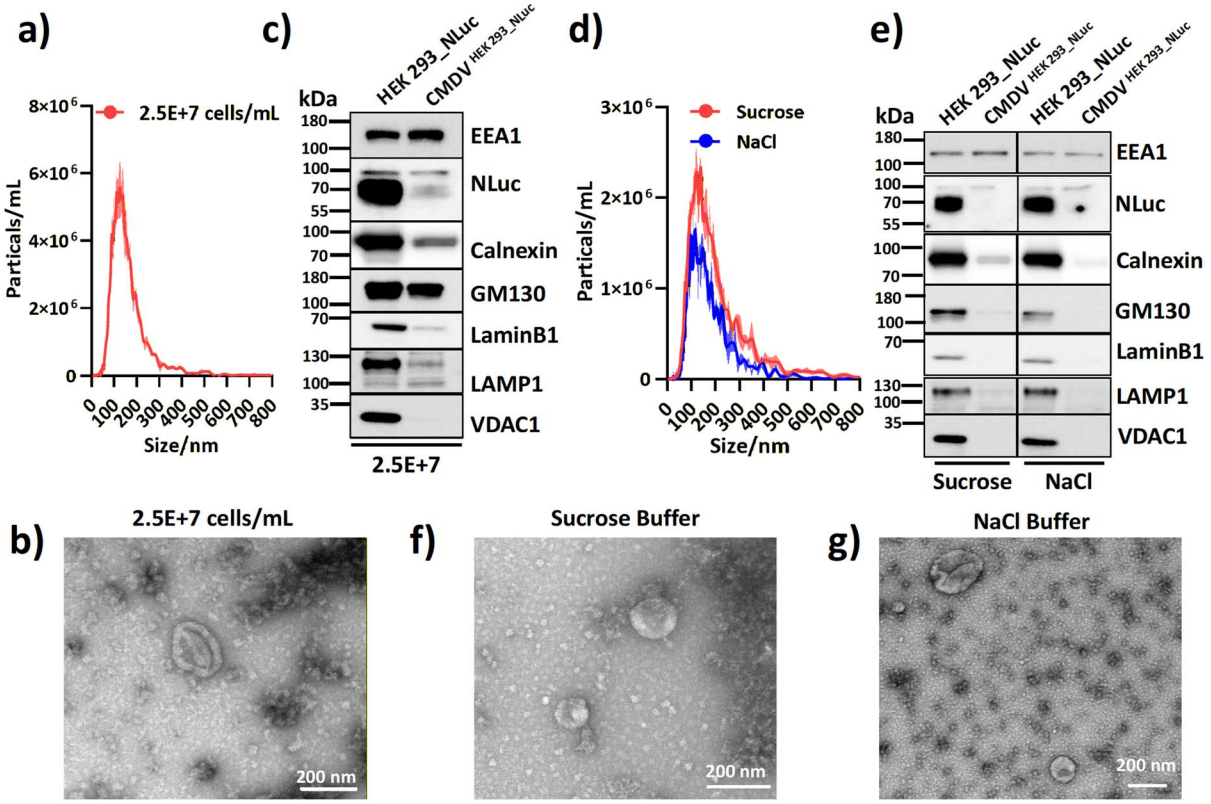

Fig. 3 Characterization of CMDVs$^{HEK\ 293_NLuc}$ produced under different cell densities and solutions. (a) The size distribution of CMDVs$^{HEK\ 293_NLuc}$ produced under a 2.5 × 10^7 cell density. (b) TEM imaging of CMDVs$^{HEK\ 293_NLuc}$ produced under a 2.5 × 10^7 cells density. (c) Western blotting of different organelle protein markers in CMDVs$^{HEK\ 293_NLuc}$ produced under a 2.5 × 10^7 cell density. (d) The size distribution of CMDVs$^{HEK\ 293_NLuc}$ produced under sucrose and NaCl buffer. (e) Western blotting of different organelle protein markers in CMDVs$^{HEK\ 293_NLuc}$ produced under sucrose and NaCl buffer. (f and g) TEM imaging of CMDVs$^{HEK\ 293_NLuc}$ produced under (f) sucrose buffer and (g) NaCl buffer. Endosome marker: EEA1, membrane protein: NLuc, ER marker: Calnexin, Golgi marker: GM130, nucleus marker: Lamin B1, lysosomal marker: LAMP1, mitochondrial marker: VDAC1.

also rose slightly (Fig. 3c). Subsequently, we examined vesicle preparation in both a high-viscosity sucrose buffer and a high-salt NaCl buffer. The size and zeta potential of the vesicles prepared under high-viscosity and high-salt conditions were essentially consistent with those prepared under mildly hypotonic buffer conditions (Fig. 3d and Table 1). Still, there is no contamination from the higher mechanical resistance organelles (Fig. 3e), but CMDVs produced under high-viscosity and high-salt conditions are almost derived from endosomes. The CMDVs also preserved a highly intact structural morphology in both high viscosity and salt buffer (Fig. 3f and g). However, the total CMDV count decreased 47% and 65% under high-viscosity and high-salt conditions, respectively (Table 1), indicating that the buffer has a significant effect on the yield and origin of vesicles.

To assess the efficiency of CMDV production, theoretical models were used to estimate the vesicle yield of CMDVs that can be generated per cell as a function of vesicle diameter (red curve), based on plasma membrane surface area, and with experimental outputs (Fig. 4). The vesicle yield of CMDVs increased with the increase of nitrogen pressures, and it is higher than the predicted yield based on the membrane area. This suggests that the method produces vesicles from diverse cellular membrane sources. Additionally, higher pressure leads to the assembly of more mechanically sensitive membrane organelles into vesicles. Furthermore, the vesicle yield of CMDVs produced under higher cell density, high-viscosity, and high-salt conditions was below the theoretical prediction, aligning with the NTA measurement results.

Together, the results suggest that the method developed for CMDV preparation *via* nitrogen cavitation is highly robust, allowing for successful CMDV generation under varying cell densities and pressures, as well as under high viscosity and ionic strength conditions. Nevertheless, it must be stressed that the membrane origin of the assembled vesicles and their yield are influenced by experimental parameters. Consequently, for effective vesicle preparation using this method, optimization of the production parameters according to the cell source and specific experimental conditions is required to produce suitable vesicles based on the downstream applications.

Functional validation of CMDVs

Since vesicles are mainly utilized for the efficient delivery of bioactive molecules, preserving their activity is a key consideration in vesicle preparation methods. To further assess vesicle integrity and functional preservation, CMDVs$^{HEK\ 293_NLuc}$ were

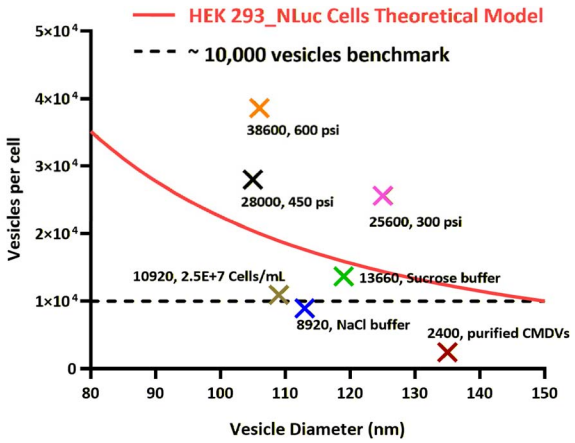

Fig. 4 Theoretical models of CMDV yield. HEK 293_NLuc cells (blue curve) were used to estimate the yield of CMDVs that can be generated per cell as a function of vesicle diameter, assuming conservation of total plasma membrane surface area. The dashed horizontal line (~10 000 vesicles per cell) represents a benchmark yield used for evaluating production efficiency. The experimental data are marked by different colored X under different experimental conditions. The specific data format is as follows: CMDV yield, experimental conditions.

purified by ultracentrifugation, followed by NLuc activity analysis (Fig. 5a). The yield of highly purified CMDVs can reach 2400 particles per cell after two ultracentrifugation steps, which indicates that the developed method enables high-yield preparation of CMDVs (Fig. 4). TEM revealed that the purified CMDVs exhibited the expected cup-shaped morphology with intact lipid bilayers, confirming high structural uniformity and membrane preservation (Fig. 5b). Notably, enzymatic assays demonstrated that NLuc activity was retained in the CMDVs after processing, indicating successful protection of membrane-bound functional proteins during cavitation and purification (Fig. 5c). To further determine whether the prepared CMDVs have the biofunction as a therapeutic system, the tumor cytotoxicity was tested using CMDVs^{CTL}. The size and the zeta potential of CMDVs^{CTL} with cup-shaped morphology are 140 nm and −35 mV, respectively (Fig. 5d and e). Western blotting confirmed that there is no contamination from mechanically robust organelles (Fig. 5f). The CMDVs^{CTL} were co-cultured with MC38-OVA cancer cells, and the cell viability was tested by flow cytometry. As shown in Fig. 5g, their killing efficiency exceeded 60% compared with the control buffer. Thus, these results indicate that CMDVs preserve the bioactive content of their donor cells and confirm their potential for producing function-preserving vesicles.

Discussion

Cell-derived vesicles are widely recognized for preserving the membrane composition and functional surface proteins of their donor cells, offering inherent biocompatibility, long circulation times, and intrinsic targeting capabilities.[20,38] However, EVs—being secreted through tightly regulated but slow biological processes—typically exhibit low yields, often requiring prolonged culture and large input volumes, which limit their scalability for preclinical and translational applications.[11,39] CMDVs can be produced directly from whole cells through a variety of physical disruption methods, offering a more rapid and scalable alternative. However, commonly used techniques, such as extrusion, sonication, freeze–thaw cycling, and homogenization, frequently subject cells to substantial mechanical or thermal stress.[40–42] These techniques can disrupt membrane architecture, create heterogeneous vesicle populations, and release intracellular components such as genomic DNA, histones, lysosomal hydrolases, and oxidative enzymes.[18,43–45] As a result, vesicle preparations frequently contain contaminants derived from nuclei, lysosomes, mitochondria, or peroxisomes, which complicate downstream functional analyses and pose challenges for standardization and safety evaluation.[46,47] These limitations highlight the need for a CMDV production platform that achieves high yield while maintaining structural selectivity and minimizing organelle-derived impurities.

Our results show that nitrogen cavitation addresses these challenges by providing controlled and selective membrane disruption. During pressure equilibration, dissolved nitrogen accumulates in both the cytosol and lipid bilayer. Rapid decompression induces microbubble nucleation and expansion, generating localized shear forces that preferentially rupture the plasma membrane, which has a lower mechanical failure threshold than nuclei, mitochondria, lysosomes, and peroxisomes. This selective disruption is consistent with the minimal levels of organelle-associated contaminants detected in our CMDV preparations. Importantly, cavitation avoids the high thermal loads and non-uniform shear commonly associated with sonication or homogenization, thereby preserving membrane protein conformation and vesicle integrity.

CMDVs generated by nitrogen cavitation retain key membrane-bound functionalities, including receptor presentation, ligand interactions, and enzymatic activity. Functional validation assays further demonstrate their capacity to enhance CTL-mediated cytotoxicity, indicating conservation of biologically relevant signaling capabilities. In addition, cavitation-derived CMDVs remain compatible with established purification workflows such as ultracentrifugation,[48] SEC,[49] and enzymatic digestion,[40] allowing integration into stringent quality-control pipelines when needed. This modularity enables downstream engineering applications, including membrane hybridization, vesicle–nanoparticle assembly, and synthetic-biology-based surface modifications.[50] Overall, the mechanistic selectivity, structural preservation, and functional retention demonstrated in this study support nitrogen cavitation as a robust and scalable strategy for CMDV generation.

Nitrogen cavitation also has inherent limitations. Rupture selectivity is cell-type dependent, as different cells exhibit distinct mechanical thresholds, requiring pressure optimization for each system. Although cavitation reduces organelle contamination, size heterogeneity can still occur, necessitating additional purification for applications requiring high uniformity. Extremely fragile or highly vacuolated cells may also experience non-selective rupture. Finally, because cavitation

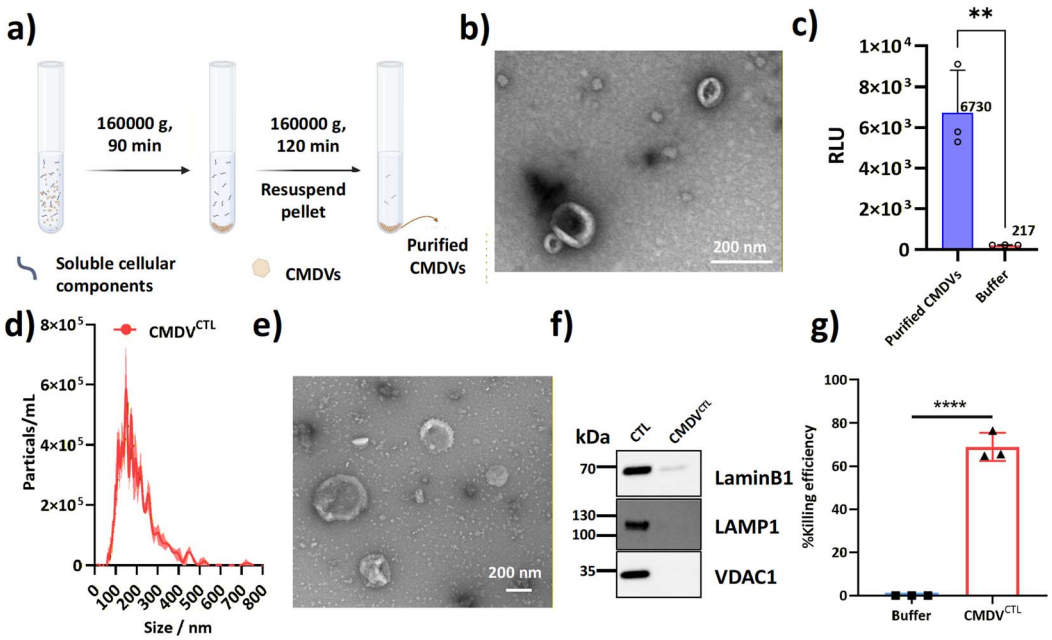

Fig. 5 Functional validation of CMDVs. (a) Schematic of CMDVs$^{HEK\ 293_NLuc}$ purification *via* ultracentrifugation. Created with Biorender.com. (b) TEM imaging of purified CMDVs$^{HEK\ 293_NLuc}$. (c) Activity analysis of NLuc in purified CMDVs$^{HEK\ 293_NLuc}$. (d) The size distribution of CMDVs^{CTL}. (e) TEM imaging of CMDVs^{CTL}. (f) Western blotting of different organelle protein markers in CMDVs^{CTL}. (g) Quantification of the killing efficiency of CMDVs^{CTL} against MC38-OVA cells.

bypasses endogenous vesicle biogenesis, it cannot be used to study natural cargo-sorting or EV secretion pathways.

Conclusion

In this study, we propose a streamlined strategy for generating CMDVs *via* nitrogen cavitation. This modularity makes the method compatible with downstream integration into bioreactor-based production systems, membrane-coating workflows, or CMDV–nanoparticle hybrid constructs. Beyond acting as delivery vehicles, CMDVs can serve as modular building blocks in a wide range of applications, including cell membrane hybridization, immune modulation, and biomimetic coatings.[50] By coupling this approach with emerging technologies in synthetic biology and drug formulation, CMDVs may be further engineered for targeted delivery, immune evasion, or biosensing functions. In conclusion, we have developed a rapid, scalable, and function-preserving method to prepare CMDVs using nitrogen cavitation. This platform enables consistent production of structurally intact and biologically active vesicles, offering a practical foundation for advancing CMDV-based therapeutics and translational applications.

Author contributions

C. Li conceived the study, designed the experiments, and performed nitrogen cavitation-based vesicle preparation with the assistance of W. Su, W. Xu, and J. Zhou. D. Luo and Q. Luo conducted biochemical assays and vesicle characterization. C. Peng performed TEM analysis. W. Wu carried out the CTL cytotoxicity assays. C. Li and Y.-F. Wang wrote the manuscript. All authors discussed the results, provided critical feedback, and contributed to the final version of the manuscript.

Conflicts of interest

There are no conflicts to declare.

Data availability

The data that support the work are available from the corresponding author upon reasonable request.

Supplementary information (SI): figures including all uncropped Western blotting images mentioned in the main text. See DOI: https://doi.org/10.1039/d5na00855g.

Acknowledgements

We thank Shuangya Chen for assistance with cell culture and nitrogen cavitation experiments. Y.-F. Wang acknowledges the National Natural Science Foundation of China (grant no. 32571616 and 32101126) and the Guangzhou Science and Technology Bureau's Basic Research Plan (G24151032). C. Li acknowledges funding support from the Newshell VesicleTech Program.

References

1 M. Yáñez-Mó, P. R. Siljander, Z. Andreu, A. B. Zavec, F. E. Borràs, E. I. Buzas, K. Buzas, E. Casal, F. Cappello, J. Carvalho, *et al.*, Biological properties of extracellular

vesicles and their physiological functions, *J. Extracell. Vesicles*, 2015, **4**, 27066.
2 C. Thery, K. W. Witwer, E. Aikawa, M. J. Alcaraz, J. D. Anderson, R. Andriantsitohaina, A. Antoniou, T. Arab, F. Archer, G. K. Atkin-Smith, *et al.*, Minimal information for studies of extracellular vesicles 2018 (MISEV2018): a position statement of the International Society for Extracellular Vesicles and update of the MISEV2014 guidelines, *J. Extracell. Vesicles*, 2018, **7**, 1535750.
3 M. Tkach, J. Kowal and C. Thery, Why the need and how to approach the functional diversity of extracellular vesicles, *Philos. Trans. R. Soc., B*, 2018, **373**, 20160479.
4 S. C. Jang, O. Y. Kim, C. M. Yoon, D. Choi, T. Roh, J. Park, J. Nilsson, J. Lötvall, Y. Kim and Y. S. Gho, Bioinspired exosome-mimetic nanovesicles for targeted delivery of chemotherapeutics to malignant tumors, *ACS Nano*, 2013, **7**, 7698–7710.
5 Q. Le, J. Lee, H. Lee, G. Shim and Y. Oh, Cell membrane-derived vesicles for delivery of therapeutic agents, *Acta Pharm. Sin. B*, 2021, **11**, 2096–2113.
6 X. Xu, L. Xu, J. Wang, C. Wen, J. Xia, Y. Zhang and Y. Liang, Bioinspired cellular membrane-derived vesicles for mRNA delivery, *Theranostics*, 2024, **14**, 3246–3266.
7 Q. Tang, X. Zhang, W. Zhang, S. Zhao and Y. Chen, Identification and characterization of cell-bound membrane vesicles, *Biochim. Biophys. Acta*, 2017, **1859**, 756–766.
8 Y. Zhang, Y. Liu, W. Zhang, Q. Tang and Y. Chen, Isolated cell-bound membrane vesicles (CBMVs) as a novel class of drug nanocarriers, *J. Nanobiotechnol.*, 2020, **18**, 69.
9 J. Z. Nordin, Y. Lee, P. Vader, I. Mäger, H. J. Johansson, W. Heusermann, O. P. B. Wiklander, M. Hällbrink, Y. Seow, J. J. Bultema, *et al.*, Ultrafiltration with size-exclusion liquid chromatography for high yield isolation of extracellular vesicles preserving intact biophysical and functional properties, *Nanomedicine*, 2015, **11**, 879–883.
10 R. J. Lobb, M. Becker, S. W. Wen, C. S. F. Wong, A. P. Wiegmans, A. Leimgruber and A. Möller, Optimized exosome isolation protocol for cell culture supernatant and human plasma, *J. Extracell. Vesicles*, 2015, **4**, 27031.
11 J. Lötvall, A. F. Hill, F. Hochberg, E. I. Buzás, D. Di Vizio, C. Gardiner, Y. S. Gho, I. V. Kurochkin, S. Mathivanan, P. Quesenberry, *et al.*, Minimal experimental requirements for definition of extracellular vesicles and their functions: a position statement from the International Society for Extracellular Vesicles, *J. Extracell. Vesicles*, 2014, **3**, 26913.
12 G. K. Patel, M. A. Khan, H. Zubair, S. K. Srivastava, M. Khushman, S. Singh and A. P. Singh, Comparative analysis of exosome isolation methods using culture supernatant for optimum yield, purity and downstream applications, *Sci. Rep.*, 2019, **9**, 5335.
13 S. Williams, M. Fernandez-Rhodes, A. Law, B. Peacock, M. P. Lewis and O. G. Davies, Comparison of extracellular vesicle isolation processes for therapeutic applications, *J. Tissue Eng.*, 2023, **14**, 20417314231174609.
14 M. P. Oksvold, A. Neurauter and K. W. Pedersen, Magnetic bead-based isolation of exosomes, *Methods Mol. Biol.*, 2015, **1218**, 465–481.
15 X. An, Y. Zeng, C. Liu and G. Liu, Cellular-Membrane-Derived Vesicles for Cancer Immunotherapy, *Pharmaceutics*, 2023, **16**, 22.
16 C. Xu, D. Ju and X. Zhang, Cell Membrane-Derived Vesicle: A Novel Vehicle for Cancer Immunotherapy, *Front. Immunol.*, 2022, **13**, 923598.
17 X. Li, Y. Wei, Z. Zhang and X. Zhang, Harnessing genetically engineered cell membrane-derived vesicles as biotherapeutics, *Extracell. Vesicles Circ. Nucleic Acids*, 2024, **5**, 44–63.
18 Y. T. Sato, K. Umezaki, S. Sawada, S. Mukai, Y. Sasaki, N. Harada, H. Shiku and K. Akiyoshi, Engineering hybrid exosomes by membrane fusion with liposomes, *Sci. Rep.*, 2016, **6**, 21933.
19 M. A. Rider, S. N. Hurwitz and D. G. J. Meckes, ExtraPEG: A Polyethylene Glycol-Based Method for Enrichment of Extracellular Vesicles, *Sci. Rep.*, 2016, **6**, 23978.
20 A. Parodi, N. Quattrocchi, A. L. van de Ven, C. Chiappini, M. Evangelopoulos, J. O. Martinez, B. S. Brown, S. Z. Khaled, I. K. Yazdi, M. V. Enzo, *et al.*, Synthetic nanoparticles functionalized with biomimetic leukocyte membranes possess cell-like functions, *Nat. Nanotechnol.*, 2013, **8**, 61–68.
21 M. J. Hunter and S. L. Commerford, Pressure homogenization of mammalian tissues, *Biochim. Biophys. Acta*, 1961, **47**, 580–586.
22 R. J. Simpson, Disruption of cultured cells by nitrogen cavitation, *Cold Spring Harb. Protoc.*, 2010, **2010**, pdb-prot5513.
23 R. M. Dowben, A. Gaffey and P. M. Lynch, Isolation of liver and muscle polyribosomes in high yield after cell disruption by nitrogen cavitation, *FEBS Lett.*, 1968, **2**, 1–3.
24 A. Z. Younis, G. G. Lavery, M. Christian and C. L. Doig, Rapid isolation of respiring skeletal muscle mitochondria using nitrogen cavitation, *Front. Physiol.*, 2023, **14**, 1114595.
25 M. Zhou and M. R. Philips, Nitrogen Cavitation and Differential Centrifugation Allows for Monitoring the Distribution of Peripheral Membrane Proteins in Cultured Cells, *J. Vis. Exp.*, 2017, **126**, 56037.
26 C. Li, *The RhoA-DIAPH3/Dia2 axis controls the formation of lipid nanodomains that are required for the activation of JAK/STAT signaling by IFN-γ*, Université Paris sciences et lettres, 2023, https://hal.science/tel-04003099.
27 J. Gao, M. Lee, X. Dong and Z. Wang, Generation of Membrane-Derived Nanovesicles by Nitrogen Cavitation for Drug Targeting Delivery and Immunization, *Methods Mol. Biol.*, 2022, **2394**, 575–589.
28 D. Choi, D. Kim, Y. Kim and Y. S. Gho, Proteomics, transcriptomics and lipidomics of exosomes and ectosomes, *Proteomics*, 2013, **13**, 1554–1571.
29 M. J. Broekman, Homogenization by nitrogen cavitation technique applied to platelet subcellular fractionation, *Methods Enzymol.*, 1992, **215**, 21–32.

30 J. W. Depierre and M. L. Karnovsky, Plasma membranes of mammalian cells: a review of methods for their characterization and isolation, *J. Cell Biol.*, 1973, **56**, 275–303.
31 M. S. Klempner, R. B. Mikkelsen, D. H. Corfman and J. André-Schwartz, Neutrophil plasma membranes. I. High-yield purification of human neutrophil plasma membrane vesicles by nitrogen cavitation and differential centrifugation, *J. Cell Biol.*, 1980, **86**, 21–28.
32 A. Sidi, J. T. Davidson, M. Behar and D. Olshwang, Spinal narcotics and central nervous system depression, *Anaesthesia*, 1981, **36**, 1044–1047.
33 Y. Fujiki, A. L. Hubbard, S. Fowler and P. B. Lazarow, Isolation of intracellular membranes by means of sodium carbonate treatment: application to endoplasmic reticulum, *J. Cell Biol.*, 1982, **93**, 97–102.
34 M. R. Philips, S. B. Abramson, S. L. Kolasinski, K. A. Haines, G. Weissmann and M. G. Rosenfeld, Low molecular weight GTP-binding proteins in human neutrophil granule membranes, *J. Biol. Chem.*, 1991, **266**, 1289–1298.
35 T. Kristián, I. B. Hopkins, M. C. Mckenna and G. Fiskum, Isolation of mitochondria with high respiratory control from primary cultures of neurons and astrocytes using nitrogen cavitation, *J. Neurosci. Methods*, 2006, **152**, 136–143.
36 H. C. Kondolf, D. A. D'Orlando, G. R. Dubyak and D. W. Abbott, Protein engineering reveals that gasdermin A preferentially targets mitochondrial membranes over the plasma membrane during pyroptosis, *J. Biol. Chem.*, 2023, **299**, 102908.
37 G. Blobel and V. R. Potter, Nuclei from rat liver: isolation method that combines purity with high yield, *Science*, 1966, **154**, 1662–1665.
38 G. Van Niel, G. D'Angelo and G. Raposo, Shedding light on the cell biology of extracellular vesicles, *Nat. Rev. Mol. Cell Biol.*, 2018, **19**, 213–228.
39 E. Willms, H. J. Johansson, I. Mäger, Y. Lee, K. E. M. Blomberg, M. Sadik, A. Alaarg, C. I. E. Smith, J. Lehtiö, S. El Andaloussi, *et al.*, Cells release subpopulations of exosomes with distinct molecular and biological properties, *Sci. Rep.*, 2016, **6**, 22519.
40 D. K. Jeppesen, A. M. Fenix, J. L. Franklin, J. N. Higginbotham, Q. Zhang, L. J. Zimmerman, D. C. Liebler, J. Ping, Q. Liu, R. Evans, *et al.*, Reassessment of Exosome Composition, *Cell*, 2019, **177**, 428–445.
41 I. Kimiz-Gebologlu and S. S. Oncel, Exosomes: large-scale production, isolation, drug loading efficiency, and biodistribution and uptake, *J. Contr. Release*, 2022, **347**, 533–543.
42 J. Wang, Z. Wang, Y. Zhong, Y. Zou, C. Wang, H. Wu, A. Lee, W. Yang, X. Wang, Y. Liu, *et al.*, Central metal-derived co-assembly of biomimetic GdTPP/ZnTPP porphyrin nanocomposites for enhanced dual-modal imaging-guided photodynamic therapy, *Biomaterials*, 2020, **229**, 119576.
43 R. E. Lane, D. Korbie, M. Trau and M. M. Hill, Purification Protocols for Extracellular Vesicles, *Methods Mol. Biol.*, 2017, **1660**, 111–130.
44 D. Nie, Z. Dai, J. Li, Y. Yang, Z. Xi, J. Wang, W. Zhang, K. Qian, S. Guo, C. Zhu, *et al.*, Cancer-Cell-Membrane-Coated Nanoparticles with a Yolk-Shell Structure Augment Cancer Chemotherapy, *Nano Lett.*, 2020, **20**, 936–946.
45 V. Chugh, K. V. Krishna and A. Pandit, Cell Membrane-Coated Mimics: A Methodological Approach for Fabrication, Characterization for Therapeutic Applications, and Challenges for Clinical Translation, *ACS Nano*, 2021, **15**, 17080–17123.
46 L. Margolis and Y. Sadovsky, The biology of extracellular vesicles: the known unknowns, *PLoS Biol.*, 2019, **17**, e3000363.
47 E. I. Buzás, E. Á. Tóth, B. W. Sódar and K. É. Szabó-Taylor, Molecular interactions at the surface of extracellular vesicles, *Semin. Immunopathol.*, 2018, **40**, 453–464.
48 A. N. Böing, E. van der Pol, A. E. Grootemaat, F. A. W. Coumans, A. Sturk and R. Nieuwland, Single-step isolation of extracellular vesicles by size-exclusion chromatography, *J. Extracell. Vesicles*, 2014, **3**, 23430.
49 A. Gámez-Valero, M. Monguió-Tortajada, L. Carreras-Planella, M. L. Franquesa, K. Beyer and F. E. Borràs, Size-Exclusion Chromatography-based isolation minimally alters Extracellular Vesicles' characteristics compared to precipitating agents, *Sci. Rep.*, 2016, **6**, 33641.
50 G. Liang, Y. Zhu, D. J. Ali, T. Tian, H. Xu, K. Si, B. Sun, B. Chen and Z. Xiao, Engineered exosomes for targeted co-delivery of miR-21 inhibitor and chemotherapeutics to reverse drug resistance in colon cancer, *J. Nanobiotechnol.*, 2020, **18**, 10.